Jurnal Tribologi 46 (2025) 236-248

MYTRIBOS Malaysian Tribology Society

Jurnal Tribologi

Website : jurnaltribologi.mytribos.org e-issn: 2289-7232

Raman analysis of graphene growth on cast iron piston ring

Farah Hannani Abd Rahman [1], Hilmi Amiruddin [1,2*], Mohd Fadzli Bin Abdollah [1,2], Nurin Wahidah Mohd Zulkifli [3], Noritsugu Umehara [4]

[1] Faculty of Mechanical Technology and Engineering, Universiti Teknikal Malaysia Melaka, MALAYSIA.
[2] Centre for Advanced Research on Energy, Universiti Teknikal Malaysia Melaka, MALAYSIA.
[3] Department of Mechanical Engineering, Faculty of Engineering, Universiti Malaya, MALAYSIA.
[4] Department of Micro-Nano Mechanical Science and Engineering, Graduate School of Engineering, Nagoya University, JAPAN.
*Corresponding author: hilmi@utem.edu.my

KEYWORDS

Renewable carbon precursors
Chemical vapor deposition
Graphene coating
Pyrolysis

ABSTRACT

This study investigates the potential of using renewable carbon sources, specifically oil palm fiber and polystyrene, to synthesize graphene coatings on cast iron piston rings through chemical vapor deposition. The work aims to explore sustainable alternatives to traditional, costly carbon precursors and address the need for eco-friendly materials that enhance engine component performance. The experimental process involved analyzing the pyrolysis behavior of oil palm fiber and polystyrene via thermogravimetric analysis to assess their suitability for graphene formation. Following this, the graphene-coated piston rings were examined using scanning electron microscopy and Raman spectroscopy to evaluate the quality, uniformity and structural properties of the graphene layer. The findings indicate that oil palm fiber demonstrated a higher pyrolysis rate, producing carbon vapor more efficiently than polystyrene, which led to a smoother and more homogeneous graphene coating. This enhanced coating quality suggests that oil palm fiber-based graphene holds significant promise for improving friction resistance and wear durability in internal combustion components, offering a sustainable path forward for automotive applications.

Received 24 March 2025; received in revised form 25 April 2025; accepted 28 April 2025.
To cite this article: Abd Rahman et al. (2025). Raman analysis of graphene growth on cast iron piston ring. Jurnal Tribologi 46, pp.236-248.

1.0 INTRODUCTION

In tribological systems, minimizing friction and wear is essential to prolonging the life and improving the performance of mechanical components. One of the most effective strategies for addressing these challenges is through the application of surface coatings. Coatings act as a protective barrier that mitigates direct contact between moving parts, thus minimizing wear, reducing energy loss due to friction, and enhancing the overall performance and durability of the components (Gao et al., 2024; Muhammad Haziq Ideris et al., 2023). The selection of appropriate coating material is crucial, as it must be specifically tailored to the operational environment and the mechanical components to ensure optimal performance.

Various coatings have been employed across multiple industries to address these challenges, including diamond-like carbon (DLC), tungsten carbide, and molybdenum disulfide. These coatings have demonstrated considerable success in extending the lifespan of components by reducing wear and friction (Chen et al., 2024; Sadeghi et al., 2023). However, even with these advancements, there is ongoing interest in finding novel materials that can further enhance the performance of critical components, such as piston rings, which are subject to extreme friction forces. Piston rings, which play a vital role in sealing the combustion chamber and regulating oil consumption, often suffer from surface deterioration due to metal-to-metal con tact with the cylinder liner. This wear, known as scuffing, can significantly shorten the lifespan of the piston ring and the engine, that is exacerbated by factors such as high temperatures and inadequate lubrication (Markut et al., 2024).

Graphene, a single layer of carbon atoms arranged in a two-dimensional honeycomb lattice, has emerged as a promising coating material in this context. It's remarkable mechanical properties, including exceptional strength, high thermal conductivity, and superior durability, make it a promising candidate for minimizing friction and wear in mechanical components, make it a strong candidate for reducing friction and wear in tribological applications (Zhang et al., 2020). The incorporation of graphene into surface coatings presents an opportunity to leverage its low friction coefficient, high strength, and excellent wear resistance, thereby providing a more durable and efficient solution for reducing friction-related wear in mechanical systems.

Chemical vapor deposition (CVD) is a common technique for depositing thin films, such as graphene, onto substrates. The chemical reaction of gaseous carbon precursors on a heated substrate involves the breakdown of the pre cursor molecules and deposition of carbon atoms that assemble into the graphitic structure of graphene (Kataria et al., 2014). For graphene synthesis, carrier gases such as argon and nitrogen are typically used to transport the precursor gases, while hydrogen is employed to facilitate the growth of graphene. The introduction of hydrocarbon gases as carbon sources has been shown to enhance the quality and uniformity of the graphene produced by CVD.

Recent advancements in graphene synthesis have explored the use of alternative carbon sources, particularly those derived from waste or renewable materials. Sharma et al. demonstrated the transformation of solid plastic waste into a high-value carbon source for graphene production, highlighting the potential for sustainable and cost-effective graphene synthesis. Building on this concept, researchers have explored the use of various solid carbon sources, including bio-based materials, to further enhance the properties and performance of graphene produced through the CVD method. These developments mark progress towards more efficient and environmentally friendly production of advanced materials such as graphene.

In this study, we investigate the feasibility of synthesizing graphene coatings on cast iron piston rings using renewable carbon feedstocks via the CVD method. Specifically, we focus on oil

palm fibre (OPF) and polystyrene (PS) as carbon sources, analyzing their pyrolysis behavior and the resulting quality of graphene coatings. The aim is to explore sustainable alternatives for graphene production while enhancing the tribological performance of piston rings, ultimately contributing to the development of more durable and efficient internal combustion engines components.

2.0 EXPERIMENTAL PROCEDURE

An atmospheric-pressure CVD was used for the synthesis of graphene, as shown in Figure 1(a). In this setup, the selected carbon sources, oil palm fiber (OPF) and polystyrene (PS), shown in Figure 2, were weighed for 3 g before being placed into Furnace 1. To determine the optimal carbon source that produces the best quality graphene, a set of three precursor samples were tested: OPF, OPF+PS and PS. The combined OPF+PS sample is prepared using a 1:1 weight ratio. Cast iron piston ring was polished using P600 grit sandpaper to remove the existing chromium coating. The polished piston ring is then cleaned in an acetone bath to eliminate any remaining polishing debris or contaminants, before being positioned in Furnace 2.

The synthesis process starts by heating the piston ring substrate to 760°C for 30 minutes to allow annealing. Upon finishing annealing, the carbon sources in Furnace 1 are heated to 900°C for a 60-minute growth phase where hydrogen gas was fed into the furnace system. To test the influence of hydrogen flow rates on the uniformity of graphene, the hydrogen gas flow rates were varied between 200-800 sccm. The gas serves to facilitate the dehydrogenation of carbon species to promote carbon diffusion and graphene formation on the piston ring. Figure 1(b) provides an outline of the CVD process.

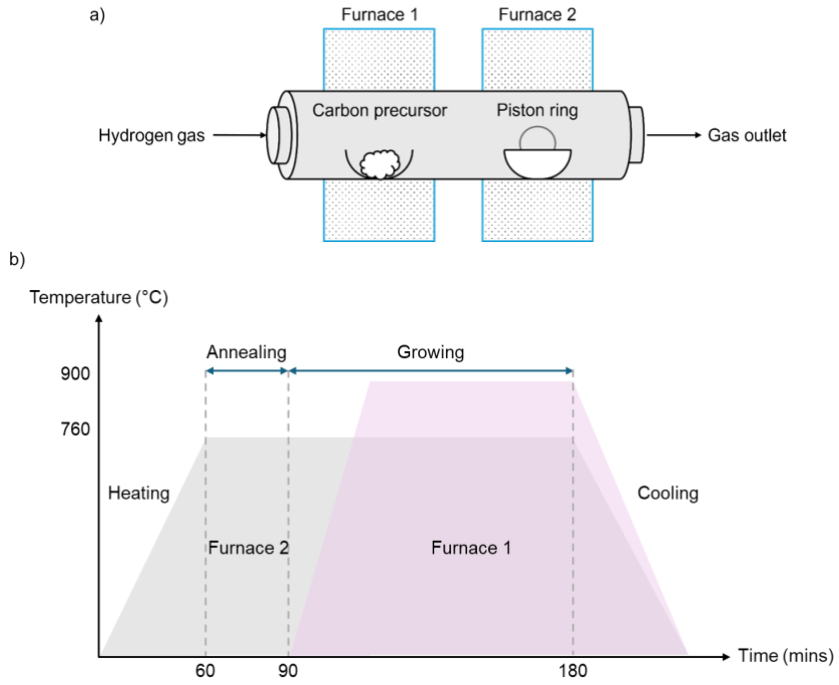

Figure 1: (a) Schematic diagram of the tube furnace for CVD process and (b) the CVD flow process.

(a) (b)

Figure 2: (a) Oil palm fiber (OPF) and (b) polystyrene (PS).

Several techniques were used to characterize the graphene-coated piston rings to verify the presence and quality of the coating. Initially, the pyrolysis rate of the carbon sources was examined using thermogravimetric analysis (TGA) using a TGA 55 Thermogravimetric Analyzer, prior to the CVD process to understand the decomposition behavior of the carbon feedstocks. Prior to the pyrolysis testing, OPF was dehydrated in an oven for 24 hours at 105°C to remove moisture and provide a basis for the TGA experiment. The polystyrene did not undergo any pre-treatment. The TGA testing parameters followed that of Chen & Lin, where 5 g of sample was analyzed at temperature range of 50-800°C where the volumetric flow rate of nitrogen gas was 100 ml min^{-1} and heating rate was 20°C min^{-2} (Chen & Lin, 2016). Nitrogen gas (N_2) is used to maintain the inert environment as well as to sweep the vapor out of the reactor (Salema & Ani, 2011). Following the CVD synthesis, the morphology of the graphene coating was evaluated using scanning electron microscopy (JEOL JSM-6010PLUS/LV SEM). The graphene-coated piston rings were characterized using Raman spectroscopy (uRaman-Ci from Technospex) to verify the presence and quality of the coating.

3.0 RESULTS AND DISCUSSION

Like other biomass, OPF is also made of cellulosic and hemi-cellulosic components along with lignin, making it a lignocellulosic biomass (Asyraf et al., 2022). According to previous studies, the thermal decomposition of lignocellulosic biomass is found to be in the range of 200-400°C where the decomposition of hemicellulose, cellulose and lignin is in the range of 200-315°C, 315-400°C and 160-900°C (Chen & Lin, 2016). The TG curve in Figure 3 revealed an initial mass loss of around 10 wt% occurring from 50 to 250°C, which indicates the removal of moisture present. The initial mass loss observed is solely attributed to the vaporisation of water molecules adsorbed on the sample surfaces and does not correspond to any pyrolytic decomposition. Therefore, this initial mass decrease is not considered part of the pyrolytic reaction process (Apaydın Varol & Mutlu, 2023). In the second stage, the high devolatisation rate from 250-400°C indicates the breakdown of hemicellulose and cellulose present in OPF. The DTG curve in the pyrolysis of OPF shows a shoulder to the left of the main degradation peak at around 250-300°C, which can be at tributed to the decomposition of hemicellulose. The highest peak at 350°C is due to the thermal degradation of cellulose. The third zone can be referred to as a lignin decomposition zone which occurs from 400°C until 800°C. From the above observations, it is concluded that the thermal decomposition of OPF mainly occurs at temperatures of 200 400°C.

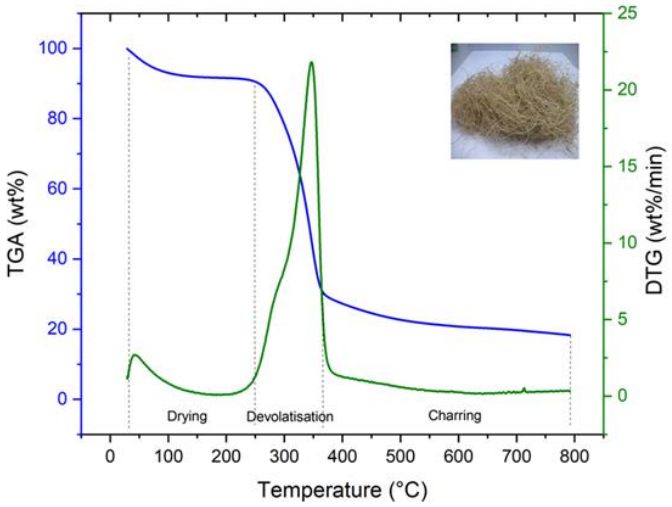

Figure 3: TG-DTG curve of oil palm fibre.

Polystyrene has a high hydrogen-carbon efficiency ratio (Sharma et al., 2014). From Figure 4, it is observed that PS undergoes rapid cracking through a single-step pyrolysis. The slight decrease observed from 200-390°C could be due to external conditions such as surface moisture or contamination before TGA testing. Also, it is known that PS, a synthetic polymer, is resistant to water due to their hydrophobic nature that prevents water absorption (Pathak & Navneet, 2017). As seen in the figure, the thermal decomposition of PS occurs at 415-500°C with a DTG peak at 480°C. This is consistent with most research studies (Singh et al., 2019; Stančin et al., 2021; Van Nguyen et al., 2021). As the temperature reached 500°C, the solid residue was reduced to 0.53 wt% at 800°C.

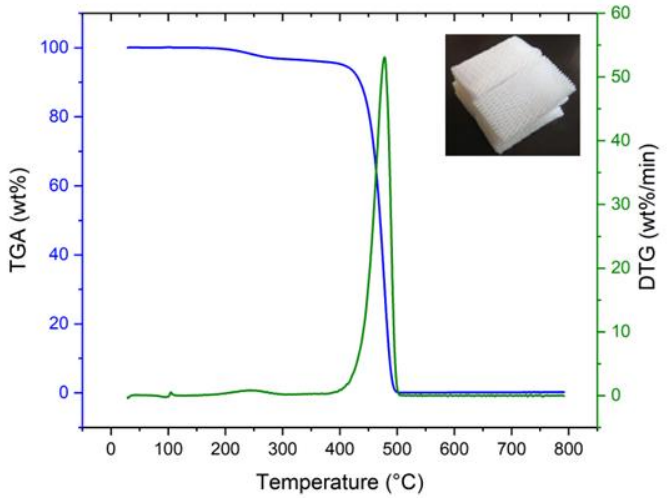

Figure 4: TG-DTG curve of polystyrene.

Figure 5 shows the combined TGA results of OPF and PS. The solid line represents OPF while the dashed line represents PS. As seen in the figure, OPF degrades at a lower temperature than PS. It can be said that OPF has a higher pyrolysis rate in a smaller temperature interval than PS.

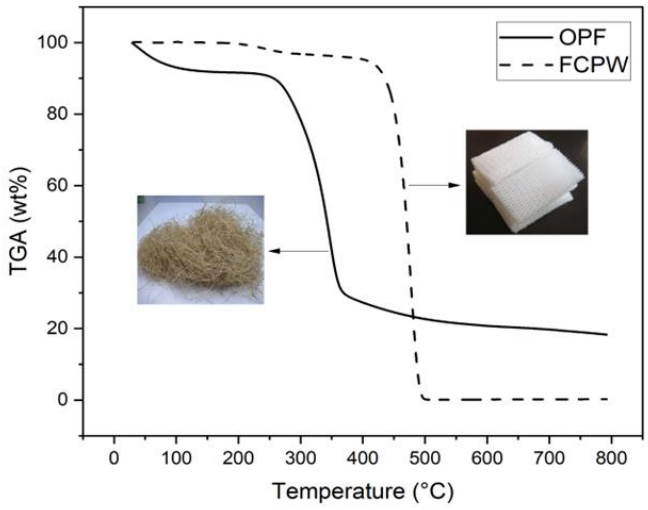

Figure 5: TGA curve of OPF (solid line) and PS (dashed line).

SEM images of the prepared graphene-coated and uncoated piston rings are presented in Figure 6. The SEM analysis of graphene coatings demonstrated distinct morphological variations based on different carbon precursors and gas flow rates. The synthesized coating 600 OPF exhibited a uniform surface with minimal porosity and no visible cracks or significant defects, forming a relatively homogeneous film layer. Similar morphologies were observed for coatings prepared with 800 OPF+PS and 800 PS; however, these samples showed contaminant particles, appearing as bright white dots, which were more prevalent in the 800 OPF coating. Coatings produced at higher gas flow rate of 800 sccm generally displayed rougher textures and increased contaminant presence, suggesting that elevated gas flow rates may contribute to reduced coating quality. In contrast, coatings such as 400 OPF, 200 OPF+PS and 600 OPF+PS displayed a coiled morphology with visible cracks, that could suggest weak bonding or stress developed during synthesis or cooling. Other than that, the irregular, dense and wavy patterns of 200 PS coatings could also indicate stress during synthesis. These findings suggest that lower gas flow rates favor the formation of more homogeneous and defect-free graphene coatings. On the other hand, at higher gas flow rates, the OPF+PS coating exhibited pronounced cracking and surface stress, whereas lower flow rates resulted in a non-uniform, uneven morphology.

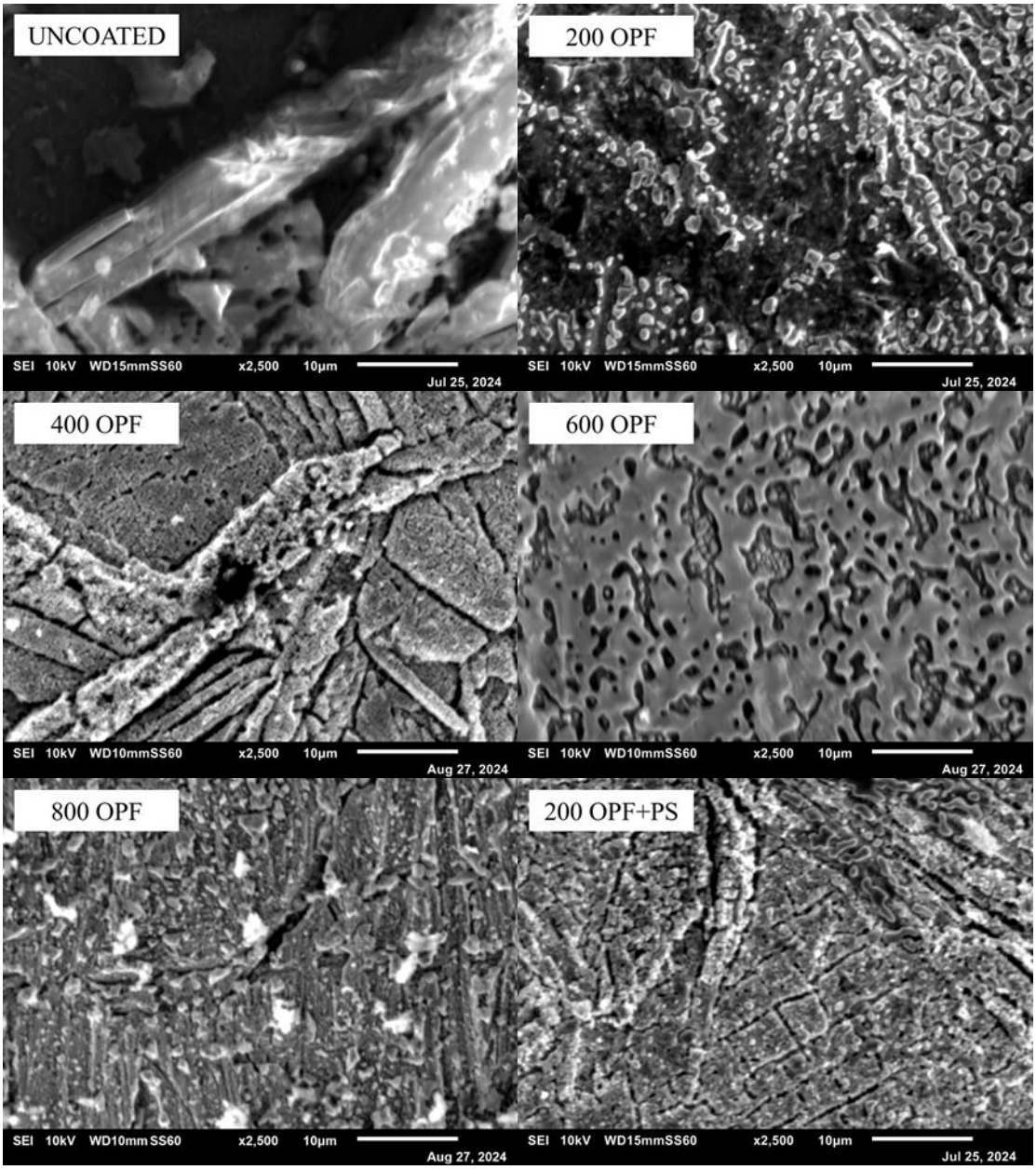
UNCOATED
SEI 10kV WD15mmSS60 x2,500 10µm
Jul 25, 2024
200 OPF
SEI 10kV WD15mmSS60 x2,500 10µm
Jul 25, 2024
400 OPF
SEI 10kV WD10mmSS60 x2,500 10µm
Aug 27, 2024
600 OPF
SEI 10kV WD10mmSS60 x2,500 10µm
Aug 27, 2024
800 OPF
SEI 10kV WD10mmSS60 x2,500 10µm
Aug 27, 2024
200 OPF+PS
SEI 10kV WD15mmSS60 x2,500 10µm
Jul 25, 2024

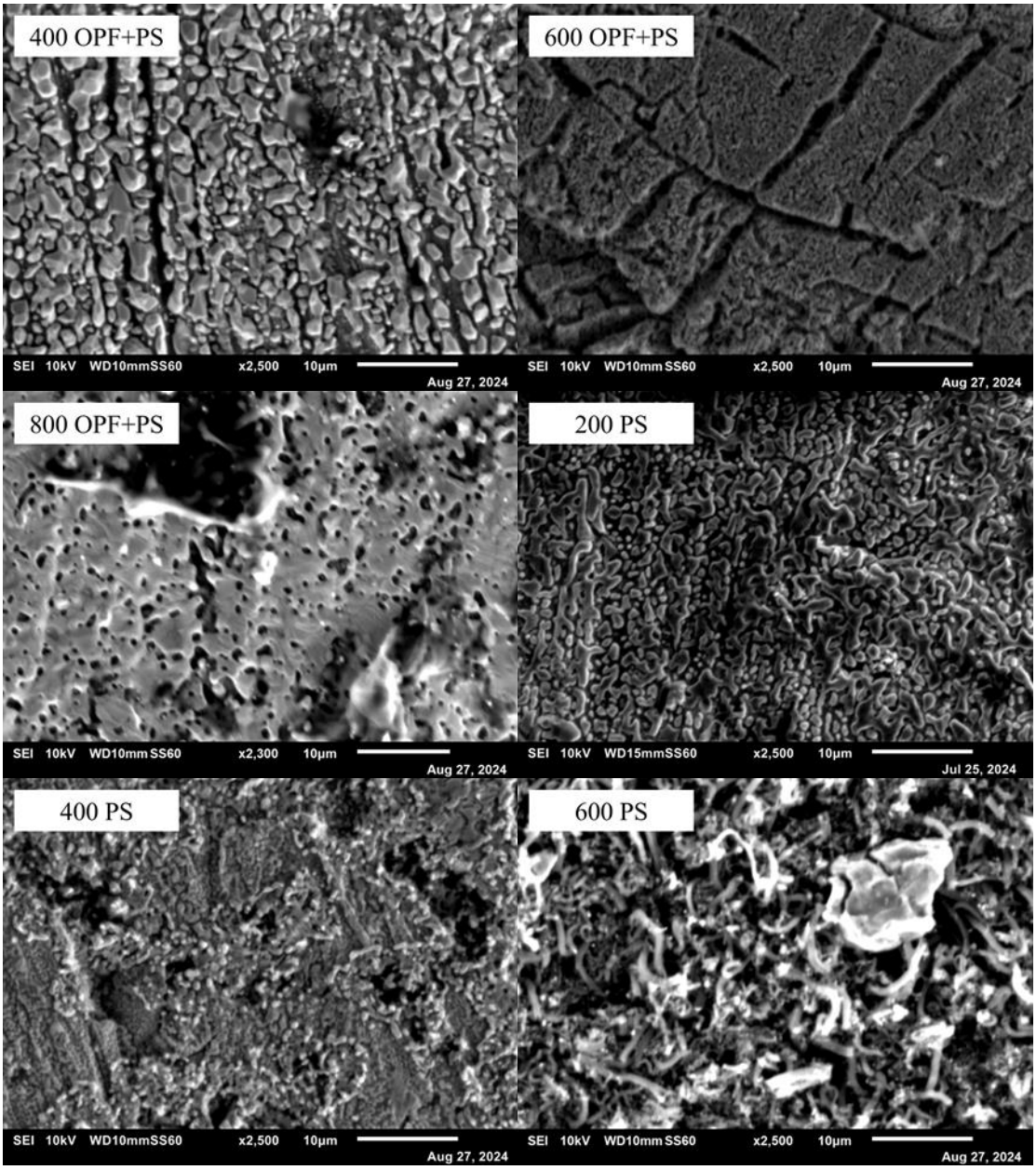
400 OPF+PS
SEI 10kV WD10mmSS60 x2,500 10µm
Aug 27, 2024
600 OPF+PS
SEI 10kV WD10mmSS60 x2,500 10µm
Aug 27, 2024
800 OPF+PS
SEI 10kV WD10mmSS60 x2,300 10µm
Aug 27, 2024
200 PS
SEI 10kV WD15mmSS60 x2,500 10µm
Jul 25, 2024
400 PS
SEI 10kV WD10mmSS60 x2,500 10µm
Aug 27, 2024
600 PS
SEI 10kV WD10mmSS60 x2,500 10µm
Aug 27, 2024

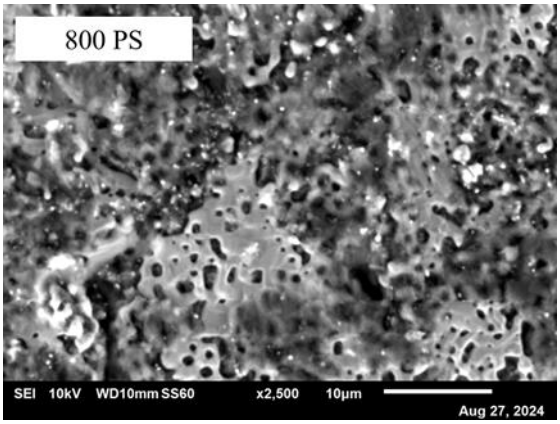

Figure 6: SEM images of graphene-coated piston ring.

Figure 7 displays the Raman spectrum of graphene grown from OPF and PS. According to studies, the D peak at around 1340-1360 cm^{-1} and G peak at around 1580-1600 cm^{-1} are indicative of the presence of graphene oxide (GO) (Wu et al., 2018). The D band is associated to the presence of defects within graphene's hexagonal carbon lattice. The ratio of the D peak intensity to the G peak intensity (I_D/I_G) is commonly used to evaluate the level of defects: a higher I_D/I_G ratio signifies more defects (Hu et al., 2023).

Table 1 displays the quantitative values derived from Raman spectrum analysis. Figure 8 shows the I_D/I_G and $FWHM_{D/G}$ ratios of synthesized graphene oxide coatings on engine piston rings using OPF, OPF+PS, and PS carbon feedstocks at varying hydrogen flow rates (200-800 sccm). The low I_D/I_G ratio observed in GO synthesized from OPF at 600 sccm suggests a reduced number of defects in the graphene lattice. Additionally, the increasing $FWHM_{D/G}$ ratio points to improved uniformity in the graphene layer, indicative of a more homogeneous graphene distribution (Rahman et al., 2023). This finding is validated by the SEM image, which shows a uniform surface with minimal porosity and no significant defects, confirming the high quality of the graphene coating.

Interestingly, GO synthesized from OPF+PS at 400 sccm stands out as an outlier among the OPF+PS group, showing the highest I_D/I_G ratio with the lowest $FWHM_{D/G}$ ratio within the same precursor series. This deviation suggests inconsistencies in carbon deposition at this particular flow rate, which potentially affects the uniformity and defect formation during the synthesis process. Conversely, PS alone shows a relatively stable but higher I_D/I_G ratios across the flow range, suggesting consistently higher structural disorder. Though coatings synthesized from PS show some uniformity based on the $FWHM_{D/G}$ values, the SEM results reveal persistent surface roughness and the presence of contaminant particles.

These results highlight that while a low I_D/I_G and high $FWHM_{D/G}$ ratio are generally desired, the relationship between defect density and coating uniformity is not always linear. The final coating characteristics are shaped by the combined effects of precursor composition, flow rate and decomposition behaviour during CVD synthesis. Notably, the combination of OPF+PS produced better outcomes than PS alone, which can be attributed to the complementary nature of the two carbon precursors. The improved Raman results are consistent with the SEM observations showing reduced contaminant presence and more uniform morphologies in OPF+PS-based coatings.

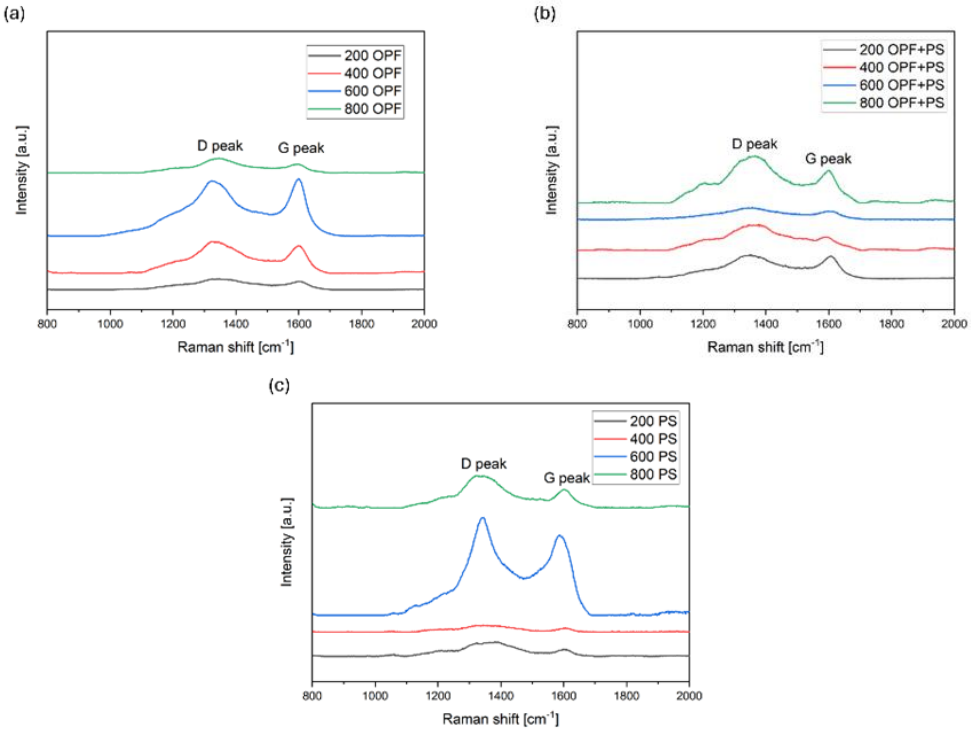

Figure 7: Raman spectrum of GO of (a) OPF, (b) OPF+PS, and (c) PS at varying hydrogen flow rates from 200 to 800 sccm.

Table 1: Raman spectrum analysis of synthesized GO coatings on engine piston ring surfaces.

Carbon precursor	**D-shift**	**G-shift**	**I_D**	**I_G**	**$FWHM_D$**	**$FWHM_G$**	**I_D/I_G**	**$FWHM_{D/G}$**
200 OPF	1351.69	1598.81	2478.75	1723.16	267.81	85.21	1.4384	3.142
400 OPF	1346.76	1596.06	7017.56	6042.66	243.12	81.02	1.1613	3.004
600 OPF	1334.67	1595.82	11629.32	12285.69	269.49	77.86	0.9465	3.461
800 OPF	1347.90	1588.53	3131.11	1893.23	217.36	97.76	1.6538	2.223
200 OPF+PS	1357.73	1602.73	1676.37	1506.66	266.37	81.81	1.1126	3.255
400 OPF+PS	1359.85	1593.48	1870.67	755.69	259.26	105.31	2.475	2.461
600 OPF+PS	1352.67	1603.14	841.98	556.55	278.19	92.48	1.512	3.007
800 OPF+PS	1355.54	1597.06	3425.75	2119.73	247.37	87.21	1.616	2.836
200 PS	1359.24	1601.04	1041.07	465.52	227.24	66.98	2.236	3.392
400 PS	1369.31	1597.85	1717.40	815.11	268.91	87.32	2.106	3.079
600 PS	1352.34	1580.03	6186.89	5843.49	188.03	109.12	1.058	1.723
800 PS	1357.03	1578.43	5364.55	4651.28	215.50	131.19	1.153	1.642

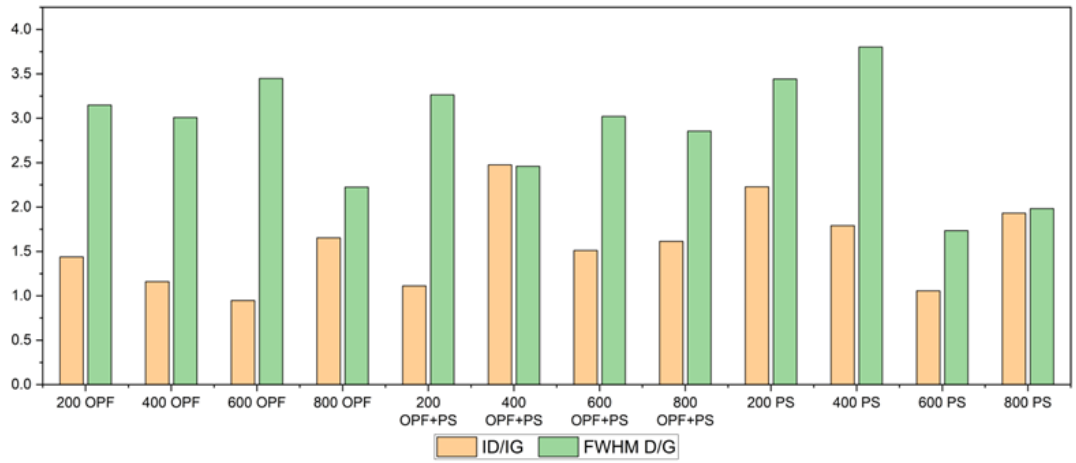

Figure 8: I_D/I_G and $FWHM_{D/G}$ ratios of synthesized GO coatings on engine piston ring surfaces.

CONCLUSIONS

In this study, the synthesis and characterization of renewably based carbon precursors were conducted. The pyrolysis rate of oil palm fiber and polystyrene were determined. It is hypothesized that the high pyrolysis rate of OPF may reduce the defect density of graphene. The synthesized graphene coating at hydrogen flow rate of 600 sccm using OPF exhibited the most uniform surface morphology with minimal defects, as confirmed by scanning electron microscopy and Raman spectroscopy analysis. Hence, it is concluded that homogeneous high-quality GO can be synthesized using OPF as carbon source through the CVD method.

ACKNOWLEDGEMENT

The authors acknowledge the usage of the facilities of Universiti Teknikal Malaysia Melaka. This research is funded by a grant from the Ministry of Higher Education Malaysia (Grant number: PT(BPKl)1000/016/018/25 Jld. 4.).

REFERENCES

Apaydın Varol, E., & Mutlu, Ü. (2023). TGA-FTIR Analysis of Biomass Samples Based on the Thermal Decomposition Behavior of Hemicellulose, Cellulose, and Lignin. Energies, 16(9), 3674. https://doi.org/10.3390/en16093674

Asyraf, M. R. M., Ishak, M. R., Syamsir, A., Nurazzi, N. M., Sabaruddin, F. A., Shazleen, S. S., Norrrahim, M. N. F., Rafidah, M., Ilyas, R. A., Rashid, M. Z. A., & Razman, M. R. (2022). Mechanical properties of oil palm fibre-reinforced polymer composites: A review. Journal of Materials Research and Technology, 17, 33–65. https://doi.org/10.1016/j.jmrt.2021.12.122

Chen, W.-H., & Lin, B.-J. (2016). Characteristics of products from the pyrolysis of oil palm fiber and its pellets in nitrogen and carbon dioxide atmospheres. Energy, 94, 569–578. https://doi.org/10.1016/j.energy.2015.11.027

Chen, Y., Li, H., Su, F., Ma, G., Li, Q., Sun, J., & Lin, S. (2024). Friction and wear behavior of molybdenum-disulfide doped hydrogen-free diamond-like carbon films sliding against Al2O3 balls at elevated temperature. Wear, 544–545, 205296. https://doi.org/10.1016/j.wear.2024.205296

Gao, R., Huang, Y., Zhou, X., Ma, G., Jin, G., Li, T., Wang, H., & Liu, M. (2024). Material system and tribological mechanism of plasma sprayed wear resistant coatings: Overview. Surface and Coatings Technology, 483, 130758. https://doi.org/10.1016/j.surfcoat.2024.130758

Hu, K., Brambilla, L., Sartori, P., Moscheni, C., Perrotta, C., Zema, L., Bertarelli, C., & Castiglioni, C. (2023). Development of Tailored Graphene Nanoparticles: Preparation, Sorting and Structure Assessment by Complementary Techniques. Molecules, 28(2), 565. https://doi.org/10.3390/molecules28020565

Kataria, S., Wagner, S., Ruhkopf, J., Gahoi, A., Pandey, H., Bornemann, R., Vaziri, S., Smith, A. D., Ostling, M., & Lemme, M. C. (2014). Chemical vapor deposited graphene: From synthesis to applications: Chemical vapor deposited graphene. Physica Status Solidi (a), 211(11), 2439–2449. https://doi.org/10.1002/pssa.201400049

Markut, T., Summer, F., Pusterhofer, M., & Grün, F. (2024). Emergence of Coated Piston Ring Scuffing Behavior on an Application-Oriented Tribological Model Test System. Lubricants, 12(6), 218. https://doi.org/10.3390/lubricants12060218

Muhammad Haziq Ideris, Shafie Kamaruddin, Mohd Hafis Sulaiman, Nor Aiman Sukindar, Ahmad Zahirani Ahmad Azhar, & Ahmad Shah Hizam Md Yasir. (2023). Effects of Coating and Lubrication on Friction and Wear for Metal-to Metal Application. Journal of Advanced Research in Applied Mechanics, 110(1), 52–62. https://doi.org/10.37934/aram.110.1.5262

Pathak, V. M. & Navneet. (2017). Review on the current status of polymer degradation: A microbial approach. Bioresources and Bioprocessing, 4(1), 15. https://doi.org/10.1186/s40643-017-0145-9

Rahman, N. L., Amiruddin, H., Abdollah, M. F. B., & Umehara, N. (2023). Synthesis and characterisation of oil palm fibre-based graphene deposited on copper aprticles for superlubricity oil additive. Jurnal Tribologi, 37, 128–141.

Sadeghi, M., Omiya, T., Fernandes, F., Vilhena, L., Ramalho, A., & Ferreira, F. (2023). Tribological Behavior of Doped DLC Coatings in the Presence of Ionic Liquid Additive under Different Lubrication Regimes. Coatings, 13(5), 891. https://doi.org/10.3390/coatings13050891

Salema, A. A., & Ani, F. N. (2011). Microwave induced pyrolysis of oil palm biomass. Bioresource Technology, 102(3), 3388–3395. https://doi.org/10.1016/j.biortech.2010.09.115

Sharma, S., Kalita, G., Hirano, R., Shinde, S. M., Papon, R., Ohtani, H., & Tanemura, M. (2014). Synthesis of graphene crystals from solid waste plastic by chemical vapor deposition. Carbon, 72, 66–73. https://doi.org/10.1016/j.carbon.2014.01.051

Singh, R. K., Ruj, B., Sadhukhan, A. K., & Gupta, P. (2019). Thermal degradation of waste plastics under non-sweeping atmosphere: Part 1: Effect of temperature, product optimization, and degradation mechanism. Journal of Environmental Management, 239, 395–406. https://doi.org/10.1016/j.jenvman.2019.03.067

Stančin, H., Šafář, M., Růžičková, J., Mikulčić, H., Raclavská, H., Wang, X., & Duić, N. (2021). Co-pyrolysis and synergistic effect analysis of biomass sawdust and polystyrene mixtures for production of high-quality bio-oils. Process Safety and Environmental Protection, 145, 1–11. https://doi.org/10.1016/j.psep.2020.07.023

Van Nguyen, Q., Choi, Y.-S., Choi, S.-K., Jeong, Y.-W., & Han, S.-Y. (2021). Co-pyrolysis of coffee-grounds and waste polystyrene foam: Synergistic effect and product characteristics analysis. Fuel, 292, 120375. https://doi.org/10.1016/j.fuel.2021.120375

Wu, J.-B., Lin, M.-L., Cong, X., Liu, H.-N., & Tan, P.-H. (2018). Raman spectroscopy of graphene-based materials and its applications in related devices. Chemical Society Reviews, 47(5), 1822–1873. https://doi.org/10.1039/C6CS00915H

Zhang, Z., Du, Y., Huang, S., Meng, F., Chen, L., Xie, W., Chang, K., Zhang, C., Lu, Y., Lin, C., Li, S., Parkin, I. P., & Guo, D. (2020). Macroscale Superlubricity Enabled by Graphene-Coated Surfaces. Advanced Science, 7(4), 1903239. https://doi.org/10.1002/advs.201903239